applied sciences

MDPI

Article

Broadband Holography via Structured Black Silicon Nano-Antennas

Mohammed Sait †, Valerio Mazzone † and Andrea Fratalocchi *

PRIMALIGHT, Faculty of Electrical Engineering; Applied Mathematics and Computational Science, King Abdullah University of Science and Technology, Thuwal 23955-6900, Saudi Arabia; mohammed.sait@kaust.edu.sa (M.S.); valerio.mazzone@kaust.edu.sa (V.M.)

* Correspondence: andrea.fratalocchi@kaust.edu.sa; Tel.: +966-(2)-8080348

† Both authors contributed equally to the work.

Received: 6 March 2019; Accepted: 27 March 2019; Published: 1 April 2019

Abstract: Computer-generated holograms have wide applications in different fields of optics, ranging from imaging, data storage, to security.Herein, we report a new method for the fabrication of large-scale computer-generated holograms from an inexpensive material, such as Silicon. Our approach exploits dry etching to create a series of broadband nanoantennas, which can tune the reflectivity of Si from an average of 0.35 to 0.1 in the entire visible range. We demonstrated the realisation of different images at wavelengths of 450 nm, 532 nm, and 632 nm with an efficiency of 10%, 14%, and 12%, respectively, thus opening up the application of large-scale broadband computer-generated holographic surfaces.

Keywords: computer-generated holograms; black silicon; broadband holography

1. Introduction

Holography has been largely exploited in a vast range of fields, such as imaging [1–5], synthetic optical elements [6], data storage [7], metrology [8], and anti-counterfeiting [9,10].

Computer-generated holograms reconstruct 2D, as well as 3D objects, calculating the required interference pattern both in the phase and amplitude based on light propagation simulations [11–14].

The recent progress in laser and computer technology allows us to fully take advantage of Computer-Generated Holograms (CGH). CGH has the capability to reconstruct 2D, as well as 3D objects by numerically generated patterns based on the intensity and phase profiles of the object that do not need to exist in reality [15–17]. Currently, the realisation of efficient and miniaturised holograms passes through complicated fabrication processes and sometimes expensive materials, such as gold, that are difficult to scale up [18–21].

In this work, we present a new efficient method to fabricate a broadband intensity binary hologram using a single inexpensive dielectric material. We leverage on the possibility to selectively turn different areas of a Si wafer into a series of Si nanoantennas, which can change the reflectivity of the Si to obtain a completely dark material [22].

This technique was inspired by the fabrication of Black Silicon BSi [23–25], that was created by patterning the entire surface of the sample. The fabrication involves a photolithography step to transfer the interference pattern on the Si sample, and a subsequent dry etching process which generates a local pattern of Si nanotips that behaves as broadband nanoantennas on specific areas of the sample. This process changes the effective refractive index of the Si, opening up the possibility of obtaining surfaces with very low reflectivity. Currently, BSi is mostly being used as a bulk material, and there have been no applications in holography.

Herein, we present our experiments in which we created different holographic images, and we show their broadband response by illuminating them with three different wavelengths from 440 nm to 632 nm. Our results enable the possibility to develop a cost-effective and large-scale platform to fabricate broadband binary amplitude holograms.

2. Material and Methods

2.1. Binary Computer Generated Hologram Algorithm

The CGH was generated using the conventional ray-tracing approach, where each object point in the 2D array is treated as a source of spherical wave, modelled by:

$$E_o = A_o \frac{exp(ikr)}{r} \tag{1}$$

where A_o is the light wave amplitude (it can take values of either 1 or zero, since it is a binary hologram), $exp(ikr)$ is the phase factor, k is the wave number, and r is the distance between the object point at the x, y plane, and x', y' parallel plane, given by:

$$r = \sqrt{(x-x')^2 + (y-y')^2 + z^2} \tag{2}$$

The z-axis was chosen to be perpendicular to the hologram, where the hologram was set at $z = 0$ and the object plane was set to $z = -60$ cm. The reference wave was chosen to be a plane wave (as it can produce clear reconstruction images), described as:

$$E_R = A_R exp(ik(x\alpha + y\beta + z\gamma)) \tag{3}$$

The total amplitude is computed by summing up all the contributions of the object wave and spherical wave at each point,

$$E_R = \sum_p \frac{A(p)exp(ikr_p)}{r_p} \tag{4}$$

where p is the index at each object point. The intensity of the total field is calculated as follows:

$$I = E_T E_T{}^* \tag{5}$$

At this stage, the intensity is a continuous representation of the interference pattern. In order to obtain a pattern suitable to be transferred onto the BSi material, binarization based on a certain threshold was applied to the intensity matrix. The CGH pattern was generated using a MATLAB platform, and the simulation parameters are set as follows: the wavelength is set to 532 nm (λ = 532 nm), hologram dimension of 3 cm × 3 cm, and sampling distance of 10 µm, which in turn leads to a pixel resolution of 3000 × 3000 pixels. The reference wave (plane wave) was designed such that it illuminates the hologram plane at a perpendicular direction. Once the hologram matrix was calculated (as the sum of the object wave and the reference wave matrices), the hologram iwass binarized in such a way that the amplitude values across the interference pattern can only assume the values of 0 or 1.

2.2. Fabrication of Binary Computer Generated Hologram

To clean the Silicon wafer, it was first submerged in Acetone, and then in Isopropyl Alcohol (IPA), and subsequently rinsed with deionised water and dried with a N_2 gun-blower. Then, a 10 µm thick layer of AZ9260 positive photo-resist was spin-coated onto the sample. The sample was then baked for 180 s at a temperature of 110 °C. The lithography process starts fabricating a chromium photomask by means of direct laser writing with a resolution of 1 µm. The Si wafer is then exposed through the

mask by Ultraviolet (UV) light with a dose value of 1800 mJ/cm^2, in order to transfer the calculated interference pattern on the Si wafer. The sample was then submerged into a developing bath using a AZ726 developer for 6 minutes. The developer removes the exposed area, leaving the sample with the desired pattern. Reactive Ion Etching was applied in order to transform the photoresist free area into black silicon. The gasses used to perform the etching procedure were O_2 and SF_6 ions, with a dose of 20 sccm each. The chamber pressure was set to 30 mtorr, with a RF power of 50 W and Inductively Coupled Plasma (ICP) power of 50 W. The recipe used was discovered through an optimisation procedure against the the following parameter, O_2 from 10 to 20 sccm keeping the SF_6 at 20 sccm, while RF power was swiped from 50 W to 100 W, and the same for the Inductively Coupled Plasma (ICP). After the etching process was concluded, the sample was exposed to UV light for 120 s. Finally, the sample was submerged again into the AZ 726 developer for 6 minutes in order to remove the rest of the photo-resist material, leaving reflecting and absorbing surfaces on the sample.

2.3. Optical Setup

The optical setup for imaging reconstruction of the fabricated CGH is illustrated in Figure 1c. In this study, the reconstruction beam was continuously illuminated by diode lasers with different wavelengths of 440 nm, 532 nm, and 632 nm, respectively. The laser source beam was collimated using a lens of 10 cm focal length, which guarantees the right beam-spot dimension. The beam then illuminates the hologram by passing through a beam-splitter in transmission. The object wavefronts were captured via the imaging screen after passing back to the beam-splitter in reflection. The reconstruction process was carried out in a darkroom. The efficiency of the BSi hologram was calculated as the ratio between the power in the holographic image and the total power illuminating the holographic plate.

3. Results

Figure 1a,b shows the concept of BSi holograms. The fabrication process starts calculating the binary amplitude interference pattern (see Materials and Methods). This is then recorded in the resist layer, on top of the Si surface, through a photolithography process. Once the sample is developed, the subsequent dry etching process generates subwavelength Si nanoantennas in the resist-free areas of the Silicon wafer.

To project the hologram image onto a screen, we illuminated the sample with a laser source of a specific wavelength. The image is formed by using the optical setup shown in Figure 1c, in which the hologram and the sample are at 90° with respect to each other.

The broadband reflectivity of the flat Si and the broadband absorbance of the BSi allows the hologram to work at different wavelengths.

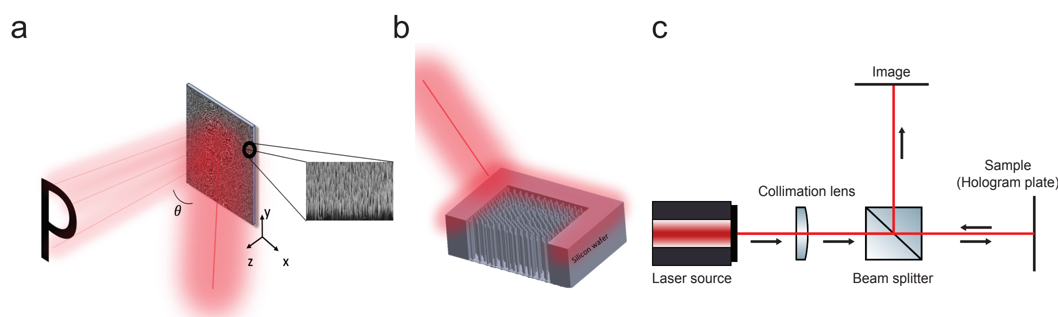

Figure 1. (**a**) Holographic reconstruction procedure and image forming by illuminating the sample with a coherent laser source. θ is the projection angle of the holographic image. (**b**) Schematic overview showing an incident laser beam reflected from the undeveloped silicon surface while the BSi region absorbs the incident light. (**c**) Optical setup used to reconstruct the hologram image.

Figure 2 shows the role of Si nanotips as nanoantennas, which enable a change of the reflectivity of the substrate from 0.35 to 0.1. In particular, Figure 2a–d shows the effect of the dry-etching time on the interference pattern realised in the sample. Figure 2e–h shows the evolution of Si nanoantennas' growth by increasing the etching time: (e) 20 min, (f) 30 min, (g) 40 min, and (h) 50 min.

Finally, Figure 2i–n plots the normalised reflectance of the structure for different etching times. The figure demonstrates the fact that the response of the structure is completely flat among all the visible wavelengths.

It can be seen that in Figure 2a for $t = 20$ min, the sample appears to be brown. This originates from the fact that at a low etching time, the Si nanotips are not yet created and the system is still reflective.

As the etching time increases, the height of pillars increases as well, reducing the reflectivity of the surface [26]. For an etching time comparable to $t = 50$ min (Figure 2h) we observe that the height of the Si nanotips starts to decrease. Another effect that appears beyond this etching time is also the etching of the protected layer, and how the sample starts to become completely black.

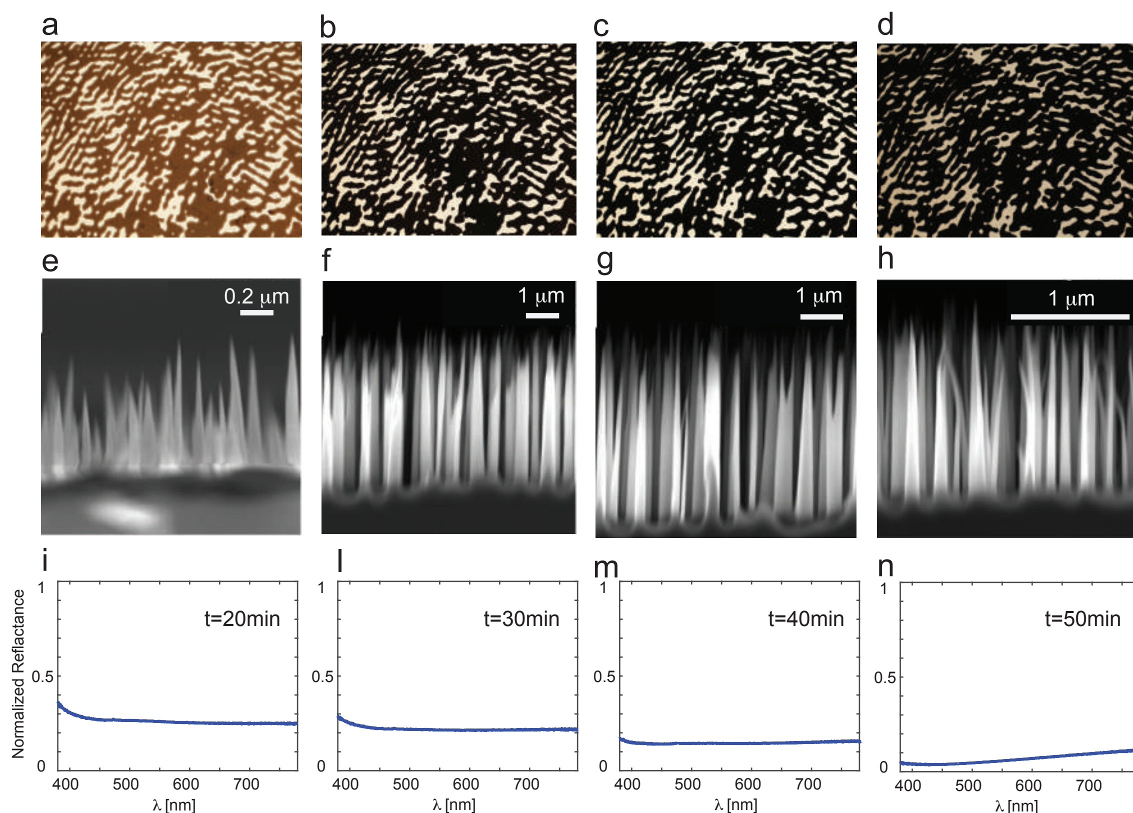

Figure 2. (**a**–**d**) Structural evolution of a BSi holographic pattern by ICP-RIE, inspected after 20 min, 30 min, 40 min, and 50 min. The pictures display the microscopic image of the fabricated holographic pattern. (**e**–**h**) Shows the cross-section SEM images of the Si nanoantennas for 20 min, 30 min, 40 min, and 50 min, respectively. (**i**–**n**) Normalised reflectance of fabricated BSi for different etching time: 20 min, 30 min, 40 min, and 50 min, respectively.

Figure 3a shows the original digital image that we chose to record for our BSi holograms, where it is composed of a sketch of the Rubiks cube with the word PRIMALIGHT. To show the large-scale possibilities of this technique and the possibility to fabricate more than one hologram at the same time, Figure 3b shows four different fabricated samples on the same Si wafer. Although the patterns are designed to work at 532 nm, all of them are able to work for multiple wavelengths. The dimension of the fabricated sample are 3 cm by 3 cm and 2 cm by 2 cm.

Figure 3c shows the numerically reconstructed image from computer simulations. Figure 3d–f shows the experimentally reconstructed images of the Rubiks cube with the word PRIMALIGHT,

using the hologram highlighted by a red circle in Figure 3b and illuminated with different wavelengths, being (d) 440 nm, (e) 532 nm, and (f) 632 nm, respectively. The reconstructed images show very good accuracy with respect to computer simulations. We calculated efficiencies for the three wavelengths of 10%, 14%, and 12%, respectively.

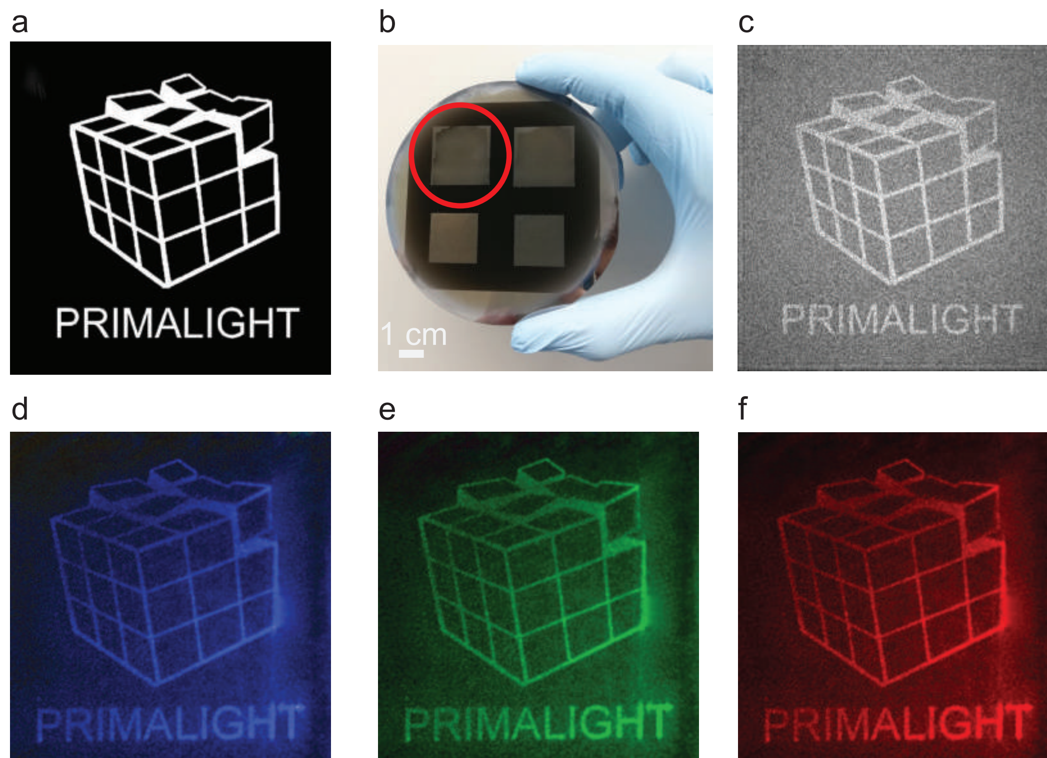

Figure 3. (**a**) Original digital image. (**b**) Four different computer generated holograms interference patterns fabricated on a single silicon wafer. (**c**) Digitally reconstructed image using the ray tracing approach. (**d**) Reconstruction using blue laser $\lambda = 450$ nm illuminating the pattern in the red circle. (**e**) Reconstruction using green laser $\lambda = 532$ nm illuminating the pattern in the red circle. (**f**) Reconstruction using red laser $\lambda = 632$ nm illuminating the pattern in the red circle.

4. Conclusions

In this work, we have demonstrated the feasibility of manufacturing binary amplitude holograms by nanostructuring Si with a controllable pattern of broadband nanoantennas.

We demonstrated this technique on a large scale, along with the simultaneous ability to manufacture a whole Si wafer and with one photolithography step.

Different techniques can also be explored within this method to transfer the interference pattern in the photoresist at a higher resolution than photolithography, including nanoimprinting, deep UV photolithography, and electron beam lithography. The intrinsic characteristic of this nanofabrication method is a fast, large-scale, and cost-effective fabrication.

This approach can also enable the realisation of holograms on flexible Silicon substrate, which can be integrated into wearable and flat electronic devices for optical imaging, data storage, and security. They can also be employed as anti-fake stamps for credit cards and currencies. Remarkably, we show that the broadband nature of the reflectivity properties of both Si and BSi allow the same hologram plate to work at different wavelengths, without observable image reconstruction losses.

Author Contributions: Conceptualization, V.M. and A.F.; methodology, V.M. and M.S.; software V.M. and M.S.; validation, V.M. and M.S.; formal analysis, V.M. and M.S.; investigation, V.M.; resources, A.F.; data curation, M.S.; writing–original draft preparation, M.S.; writing–review and editing, V.M.; visualization, V.M.; supervision, A.F.; project administration, A.F.; funding acquisition, A.F.

Funding: This research was funded by CFR-KAUST grant number OSR-2016-CRG5-2995 and The APC was funded by KAUST.

Conflicts of Interest: The authors declare no conflict of interest.

Abbreviations

The following abbreviations are used in this study:

CGH	Computer generated holograms
BSi	Black silicon
RIE	Reactive ion etching
DLW	Digital laser writer
UV	Ultraviolate
ICP	Inductive coupling power
EBL	Electron beam lithography

References

1. Yoshikawa, H.; Yamaguchi, T. Computer-generated holograms for 3D display. *Chin. Opt. Lett.* **2009**, *7*, 1079–1082.
2. Jendral, A.; Bräuer, R.; Bryngdahl, O. Computer-generated image holograms for 3D-display. *Opt. Rev.* **1995**, *2*, 187–188. [CrossRef]
3. Sando, Y.; Satoh, K.; Kitagawa, T.; Kawamura, M.; Barada, D.; Yatagai, T. Super-wide viewing-zone holographic 3D display using a convex parabolic mirror. *Sci. Rep.* **2018**, *8*, 11333. [CrossRef] [PubMed]
4. Bernhardt, M.; Nicolas, J.D.; Osterhoff, M.; Mittelstädt, H.; Reuss, M.; Harke, B.; Wittmeier, A.; Sprung, M.; Köster, S.; Salditt, T. Correlative microscopy approach for biology using X-ray holography, X-ray scanning diffraction and STED microscopy. *Nat. Commun.* **2018**, *9*, 3641. [CrossRef] [PubMed]
5. Ballard, Z.S.; Zhang, Y.; Ozcan, A. Off-axis holography and micro-optics improve lab-on-a-chip imaging. *Light Sci. Appl.* **2017**, *6*, e17105. [CrossRef] [PubMed]
6. Arnold, S.M. How to test an asphere with a computer generated hologram. In *Holographic Optics: Optically and Computer Generated*; International Society for Optics and Photonics: Los Angeles, CA, USA, 1989; Volume 1052, pp. 191–198.
7. Dhar, L.; Curtis, K.; Fäcke, T. Holographic data storage: Coming of age. *Nat. Photonics* **2008**, *2*, 403. [CrossRef]
8. Wyant, J.; Bennett, V. Using computer generated holograms to test aspheric wavefronts. *Appl. Opt.* **1972**, *11*, 2833–2839. [CrossRef]
9. Ruffato, G.; Rossi, R.; Massari, M.; Mafakheri, E.; Capaldo, P.; Romanato, F. Design, fabrication and characterization of Computer Generated Holograms for anti-counterfeiting applications using OAM beams as light decoders. *Sci. Rep.* **2017**, *7*, 18011. [CrossRef]
10. De Santis, M.; Spagnolo, G.S. Asymmetric Cryptography as subset of digital hologram watermarking. In Proceedings of the 2006 14th European Signal Processing Conference, Florence, Italy, 4–8 September 2006; pp. 1–5.
11. Wang, L.; Kruk, S.; Tang, H.; Li, T.; Kravchenko, I.; Neshev, D.N.; Kivshar, Y.S. Grayscale transparent metasurface holograms. *Optica* **2016**, *3*, 1504–1505. [CrossRef]
12. Burch, J.; Wen, D.; Chen, X.; Di Falco, A. Flexible Metasurface Holograms. *arXiv* **2016**, arXiv:1611.09537.
13. Khorasaninejad, M.; Ambrosio, A.; Kanhaiya, P.; Capasso, F. Broadband and chiral binary dielectric meta-holograms. *Sci. Adv.* **2016**, *2*, e1501258. [CrossRef] [PubMed]
14. Jin, L.; Dong, Z.; Mei, S.; Yu, Y.F.; Wei, Z.; Pan, Z.; Rezaei, S.D.; Li, X.; Kuznetsov, A.I.; Kivshar, Y.S.; et al. Noninterleaved Metasurface for (26-1) Spin-and Wavelength-Encoded Holograms. *Nano Lett.* **2018**, *18*, 8016–8024. [CrossRef] [PubMed]
15. Tsang, P.; Poon, T.C.; Wu, Y. Review of fast methods for point-based computer-generated holography. *Photonics Res.* **2018**, *6*, 837–846. [CrossRef]
16. Zhao, Y.; Cao, L.; Zhang, H.; Kong, D.; Jin, G. Accurate calculation of computer-generated holograms using angular-spectrum layer-oriented method. *Opt. Express* **2015**, *23*, 25440–25449. [CrossRef] [PubMed]
17. Jia, J.; Si, J.; Chu, D. Fast two-step layer-based method for computer generated hologram using sub-sparse 2D fast Fourier transform. *Opt. Express* **2018**, *26*, 17487–17497. [CrossRef] [PubMed]

18. Zheng, G.; Mühlenbernd, H.; Kenney, M.; Li, G.; Zentgraf, T.; Zhang, S. Metasurface holograms reaching 80% efficiency. *Nat. Nanotechnol.* **2015**, *10*, 308. [CrossRef] [PubMed]
19. Wang, B.; Dong, F.; Li, Q.T.; Yang, D.; Sun, C.; Chen, J.; Song, Z.; Xu, L.; Chu, W.; Xiao, Y.F.; et al. Visible-frequency dielectric metasurfaces for multiwavelength achromatic and highly dispersive holograms. *Nano Lett.* **2016**, *16*, 5235–5240. [CrossRef] [PubMed]
20. Yue, Z.; Xue, G.; Liu, J.; Wang, Y.; Gu, M. Nanometric holograms based on a topological insulator material. *Nat. Commun.* **2017**, *8*, 15354. [CrossRef] [PubMed]
21. Zhang, H.; Zhao, Y.; Cao, L.; Jin, G. Fully computed holographic stereogram based algorithm for computer-generated holograms with accurate depth cues. *Opt. Express* **2015**, *23*, 3901–3913. [CrossRef]
22. Hsu, C.H.; Wu, J.R.; Lu, Y.T.; Flood, D.J.; Barron, A.R.; Chen, L.C. Fabrication and characteristics of black silicon for solar cell applications: An overview. *Mater. Sci. Semicond. rocess.* **2014**, *25*, 2–17. [CrossRef]
23. Juntunen, M.A.; Heinonen, J.; Vähänissi, V.; Repo, P.; Valluru, D.; Savin, H. Near-unity quantum efficiency of broadband black silicon photodiodes with an induced junction. *Nat. Photonics* **2016**, *10*, 777. [CrossRef]
24. Savin, H.; Repo, P.; Von Gastrow, G.; Ortega, P.; Calle, E.; Garín, M.; Alcubilla, R. Black silicon solar cells with interdigitated back-contacts achieve 22.1% efficiency. *Nat. Nanotechnol.* **2015**, *10*, 624. [CrossRef] [PubMed]
25. Roy, A.B.; Dhar, A.; Choudhuri, M.; Das, S.; Hossain, S.M.; Kundu, A. Black silicon solar cell: analysis optimization and evolution towards a thinner and flexible future. *Nanotechnology* **2016**, *27*, 305302. [PubMed]
26. Steglich, M.; Käsebier, T.; Zilk, M.; Pertsch, T.; Kley, E.B.; Tünnermann, A. The structural and optical properties of black silicon by inductively coupled plasma reactive ion etching. *J. Appl. Phys.* **2014**, *116*, 173503. [CrossRef]

© 2019 by the authors. Licensee MDPI, Basel, Switzerland. This article is an open access article distributed under the terms and conditions of the Creative Commons Attribution (CC BY) license (http://creativecommons.org/licenses/by/4.0/).